Dynamic workspace reindexing using an ergonomics-based multimodal controller in teleoperation

Thijs Exterkate

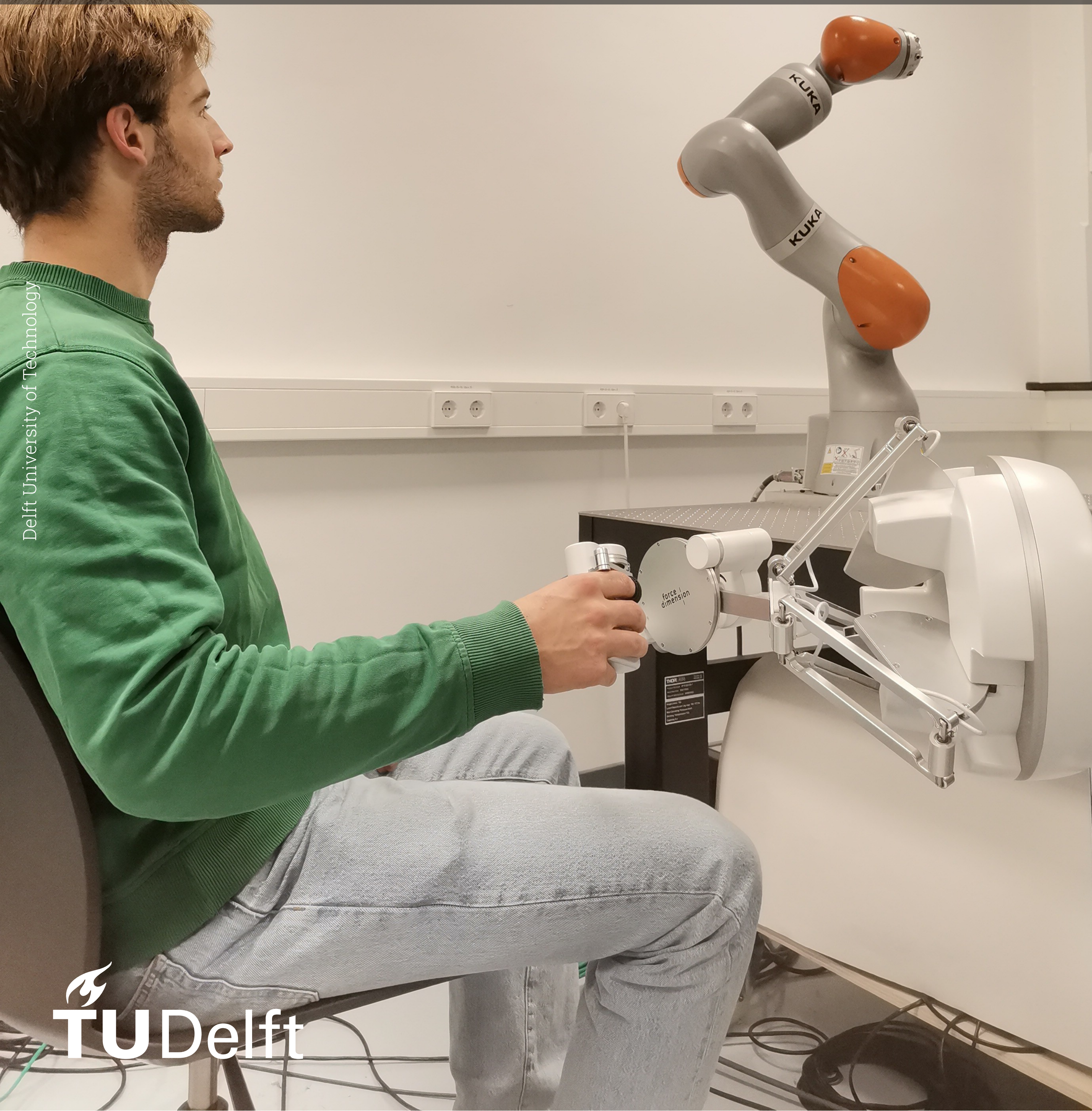

Delft University of Technology

TU Delft

Dynamic workspace reindexing using an ergonomics-based multimodal controller in teleoperation

by

Thijs Exterkate

To obtain the degree of Master of Science
at the Delft University of Technology,
to be defended publicly on Thursday March 13, 2025 at 12:00.

Student number:	4977521	
Project duration:	March, 2024 – March, 2025	
Thesis committee:	Dr. L. (Luka) Peternel,	TU Delft, supervisor
	Ir. N. (Nicky) Mol,	TU Delft, supervisor
	Dr. M. (Michaël) Wiertlewski,	TU Delft

An electronic version of this thesis is available at http://repository.tudelft.nl/.

TU Delft

Preface

This past year has been an exciting journey into robotics, centered around teleoperation. As I expected the graduation project to be a challenge, I am happy to say that it has been an enjoyable time; which I consider an achievement in itself. It was nice to work directly in the lab with actual robots, making it a hands-on and practical project.

At the core of this research is an ergonomics-based multimodal controller for dynamic workspace reindexing. Exploring this concept throughout the project has been a rewarding experience. It provided me with the opportunity to integrate theory into practice by working with a teleoperation setup, where I controlled an industrial KUKA robot using a Sigma.7 haptic device. Working on workspace reindexing, haptic feedback, and ergonomics allowed me to further develop my skills in the field of robotics. Furthermore, the freedom to choose my own project direction led me to work with a depth camera. Implementing a pose detection algorithm using the depth camera was fun and helped me acquire new skills. Connecting all the pieces and seeing the system evolve and improve over time made this an engaging project.

I would like to express my thanks to Luka and Nicky for their valuable feedback and guidance throughout this project. A huge thanks also goes to my girlfriend, family, friends, and roommates for the endless coffee moments, conversations, and support, whether it was about studies or just life in general. Looking back, I'm proud of what I've accomplished, and I definitely wouldn't be where I am today without their help.

Thijs Exterkate
Delft, March 6, 2025

Summary

To address both workspace limitations and operator ergonomics, this research proposes an ergonomics-based multimodal controller for dynamic workspace reindexing. The proposed controller interactively leverages pose and velocity control, selecting the appropriate control mode based on a ergonomic model to improve operator ergonomics.

An Ergonomic Workspace (EW) is defined based on the operator's posture. The EW is determined using an ergonomic model, ensuring that as long as the operator remains within it, their posture remains ergonomic. Control mode selection depends on the boundaries of the EW: when the operator pushes the leader handle beyond the EW boundaries, velocity control is activated. During velocity control, haptic forces/torques are generated at the leader handle to guide the operator back towards the EW. The operator can resist the haptic forces to provide the follower robot with a translational and/or rotational velocity proportional to the force/torque exerted by the operator. Commanding a constant follower velocity while maintaining a fixed leader pose enables to dynamically reindex the follower's workspace, overcoming workspace limitations. When the operator moves within the boundaries of the EW, pose control is activated. During this control mode. The operator sets the reference pose directly using the leader device. This mode offers intuitive steering and high precision, making it ideal for object interaction tasks. Since this control mode is in effect when the leader is located within the EW, an ergonomic posture is maintained during object interaction.

The proposed teleoperation system is evaluated through a teleoperation task performed using a conventional controller and the proposed controller. It is shown that the proposed controller enables to enhance ergonomics of the operator. By dynamically reindexing the workspace toward target objects, it is ensured that object interactions are consistently performed from an ergonomic posture. Furthermore, dynamic reindexing successfully addresses workspace limitations without requiring clutching or scaling.

Contents

Scientific Paper

Dynamic workspace reindexing using an ergonomics-based multimodal controller in teleoperation

Thijs Exterkate
March 6, 2025

***Abstract*—This paper proposes a multimodal controller that interactively leverages pose and velocity control for teleoperation, designed to address workspace limitations by dynamic workspace reindexing while taking into account operator ergonomics. Dynamic workspace reindexing offers a solution to the limitations of existing approaches, such as scaling and clutching. To ensure operator ergonomics, The Rapid Upper Limb Assessment (RULA) method is used to define an Ergonomic Workspace (EW) within which the operator must remain to maintain an ergonomic posture. Within the boundaries of the EW, non-scaled pose control is used to control the follower, offering intuitive interaction with the remote environment while maintaining good operator ergonomics. Outside the EW boundaries, velocity control is applied, where the velocity of the follower is based on the force exerted by the operator on the leader haptic device, allowing the operator to dynamically reindex the follower workspace. This control mode facilitates coarse positioning of the follower between targets. A proof-of-concept demonstration shows that the proposed controller succesfully addresses workspace limitations by dynamically reindexing the follower's workspace towards target objects. Furthermore, it is shown that the controller consistently maintains good operator ergonomics during interaction with the remote environment, thereby making it a suitable option for prolonged teleoperation tasks.**

I. Introduction

DRIVEN by labor shortages, advanced capabilities, and lower costs, robots are increasingly being adopted and will see greater use in the future [1]. In structured environments like the automotive industry, robots achieve higher efficiency than human employees due to their consistency, precision and resistance to fatigue [2]. However, developing robots for unstructured environments is challenging due to the complexity of understanding these environments [3]. In such cases, keeping a human in the loop for error handling remains required. However, in dangerous, toxic, or constrained environments, humans cannot be present, requiring the use of remotely operated robots [4, 5]. This has increased the demand for remotely operated robots in areas such as disaster response [6]. An example is Boston Dynamics' Spot robot, which is used in emergency cases like suspicious package cleanup [7, 8]. Other applications include remote maintenance of nuclear fusion reactors [9], nuclear waste cleanup [10], and surgery [11, 12]. This form of robot control is referred to as teleoperation or telemanipulation [13, 14].

Typically, a human would hold a tool to manipulate their environment, known as 'direct control.' In teleoperation, however, the operator uses an interface to perform these manipulations [15, 16]. This interface can vary widely, ranging from a simple joystick [17] to more complex devices, such as a data glove [18, 19].

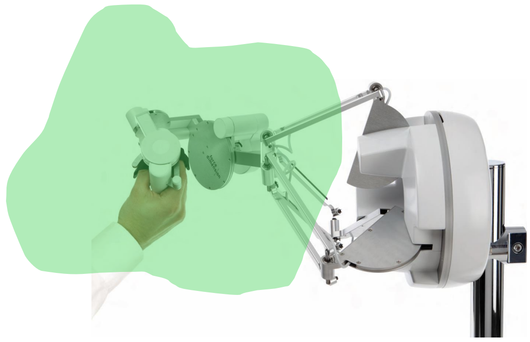

(a) Leader workspace: The operator can freely move the leader handle within the boundaries of the leader, denoted by the green area. The physical limits of the leader device restrict the operator from moving beyond the green area.

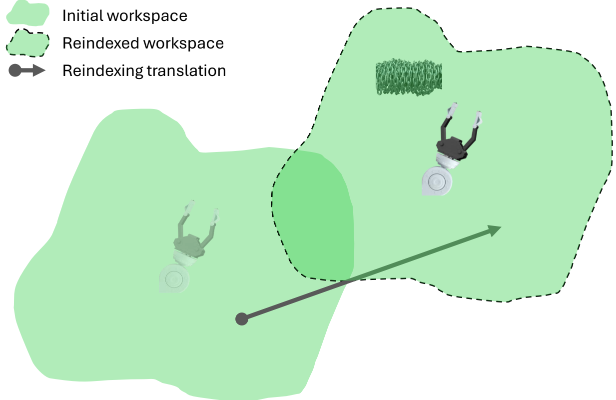

(b) Initial and reindexed follower workspace.

Fig. 1: In a conventional pose controlled teleoperation setup, the initial leader workspace can be too small to reach the target in the follower workspace. Reindexing relocates the follower workspace, enabling the gripper to reach the target.

As the range of the leader device is often limited, operating in large remote environments becomes a challenge [20]. As shown in Figure 1, the target object is beyond the reach of the follower's workspace, making it impossible to move the follower robot to the desired location. One solution is scaling, which enlarges the workspace but reduces resolution, making precise manipulation harder [21, 22, 23]. Another approach is workspace reindexing (or decoupling/clutching) [24, 25, 26], which is similar to lifting and relocating a computer mouse when it reaches the edge of the desk. However, unlike a mouse, most haptic interfaces are grounded [27, 28], so clutching requires temporarily ”freezing” the teleoperation.

Another method for enlarging follower workspace is dynamic workspace reindexing, which eliminates the need to freeze the teleoperation by using a multimodal pose/velocity control system [29, 30]. Pose control provides high fidelity and intuitive steering for precise interaction with the remote environment [31], while velocity control facilitates coarse positioning between desired locations. In this multimodal system, workspace boundaries remain fixed during pose control. While velocity control continuously shifts them towards the operator's target without having to freeze the teleoperation as in clutching.

Along with workspace challenges, teleoperation systems should consider operator posture ergonomics, as prolonged arm extension or awkward arm configurations can lead to discomfort and muscle fatigue [32, 33]. Teleoperation systems that encourage natural arm configurations improve both comfort and arm movement efficiency [34, 35]. Previous studies have emphasized the importance of incorporating postural ergonomics into teleoperation designs, as doing so can significantly improve overall system performance [36, 37, 38] and increase user acceptance [39, 40, 41].

To account for ergonomics during teleoperation, operator posture must be quantified in ergonomic terms. Various ergonomic models exist for quantifying the ergonomics of human postures. Two widely used ergonomic models are the Rapid Entire Body Assessment (REBA) [42] and the Rapid Upper Limb Assessment (RULA) [43], which are relatively simple as they primarily rely on the positions of body keypoints such as the shoulders, elbows, hips, and knees. More advanced ergonomic models incorporate musculoskeletal modeling [44, 45], which may offer enhanced accuracy but require more complex implementation. Alternatively, sensor-based approaches, such as electromyography [46], can be employed to achieve a more detailed ergonomic assessment.

To address both workspace limitations and operator ergonomics, this research proposes an ergonomics-based multimodal controller for dynamic workspace reindexing. The proposed controller interactively leverages pose and velocity control, selecting the appropriate control mode based on a ergonomic model to improve operator ergonomics.

An Ergonomic Workspace (EW) is defined based on the operator's posture. The EW is determined using an ergonomic model, ensuring that as long as the operator remains within it, their posture remains ergonomic. Control mode selection depends on the boundaries of the EW: when the operator pushes the leader handle beyond the EW boundaries, velocity control is activated, allowing the operator to dynamically reindex the workspace toward other areas of interest. Inside the ergonomic workspace (EW) boundaries, pose control allows for precise object interaction while maintaining an ergonomic body posture. As object interaction activities can typically last for extended periods, this study focuses on ensuring operator ergonomics during these tasks in particular. In contrast, dynamic workspace reindexing periods are less interesting because they are used for coarse positioning and are relatively brief.

Following research question is composed for the development of the teleoperation system:

→ **Research question:** How to develop an ergonomics-based multimodal controller that can dynamically reindex the workspace to address both workspace limitations and operator ergonomics in teleoperation?

Objectives:

1) Create an EW quantification module that incorporates a postural ergonomics model.
2) Develop a multimodal controller that interactively leverages pose and velocity control to dynamically reindex the EW.
3) Validate the proposed method using a proof-of-concept demonstration.

II. METHODS

Figure 2 illustrates the proposed teleoperation system. The light-green block represents the ergonomic model, which calculates the Ergonomic Workspace (EW) that serves as input for the controller. The dark-green block represents the proposed multimodal controller, which alternates between pose and velocity control based on the EW. Pose control is used when the leader handle is within the EW, while velocity control, allowing dynamic workspace reindexing, is used when it is outside.

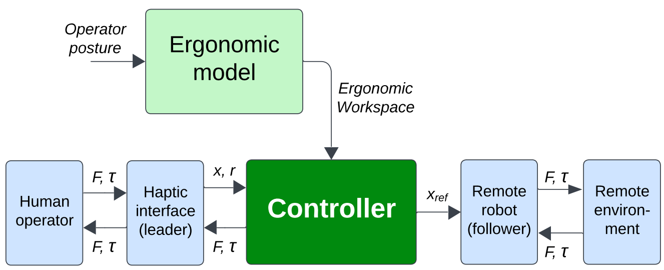

Fig. 2: Block diagram of the teleoperation system. Light blue blocks are the standard channels in a 4-channel teleoperation system. The ergonomic model computes the Ergonomic Workspace (EW) based on the operator's posture using a postural ergonomics model. The controller determines the follower reference using either pose or velocity control, depending on which control mode is currently in effect

A. Ergonomic model

The operator's posture is quantified using the Rapid Upper Limb Assessment (RULA) method [43], which assigns a score from 1 (optimal ergonomic posture, minimal injury risk) to 9 (poor posture, high injury risk). While the complete RULA method assesses the arm, hand, neck, and torso, this study focuses exclusively on the operator arm's ergonomic score. **Appendix A.1 and A.2** show how RULA is adapted for this research. The objective is to maintain a RULA score of 1 for the operator's arm throughout the teleoperation task. To achieve this, an Ergonomic Workspace (EW) is defined, ensuring that the operator's arm posture remains ergonomic (RULA=1) as long as they remain within the EW. The EW consists of both a translational component and a rotational component:

1) Translational EW: A standard arm model consists of seven Degrees of Freedom (DoF) [47, 48, 49], comprising three at the shoulder, one at the elbow, and three at the wrist. To determine the translational EW, we calculate all possible wrist positions by iterating over the three shoulder DoF's and the elbow DoF. Each arm configuration is assigned a RULA score. This generates a database of ergonomic scores for all possible arm configurations, as shown in Figure 3a. RULA scores of 7, 8 and 9 are not observed in this study, as rules regarding movement repetitiveness, operator muscle force and shoulder elevantion are not considered in the analysis. Arm configurations with a RULA score of 1 are filtered to form a 3D body that encloses all wrist positions associated with a RULA score of 1, designated as the Ergonomic Workspace (EW), see Figure 3b. To maintain an ergonomic posture, the operator must remain within the translational EW boundaries. Figure 3b also shows an example of an arm configuration within the EW, corresponding to a RULA score of 1. It should be noted that the three DoF's at the wrist are neglected for simplicity. A detailed elaboration on how the operator arm is modelled to determine the translational EW is shown in **Appendix A.3**.

2) Rotational EW: In addition to the translational EW, a rotational EW is defined. The boundaries of the rotational EW are $[-15, 15]$ degrees for pitch, roll, or yaw, as specified by RULA for wrist rotations. These limits are applied to the leader handle, so if the leader handle's rotation in any of the three rotational directions exceeds 15 degrees, the pose is considered outside the rotational EW.

B. Controller

The proposed controller alternates between two control modes: pose-pose control, where the leader handle's pose is used as a reference for the follower robot, and force-velocity control, where the operator's applied force on the leader handle dictates the reference velocity for the follower. The following paragraphs explain both control modes, with pseudocode provided in Figure 4.

- **Control Mode 1 (Pose Control)**: In this mode, the operator sets the reference pose (both position and rotation) using the leader device. The follower robot follows the reference pose set by the leader. This control mode is activated when the the leader handle is located within the ergonomic workspace (EW), either within the EW boundaries shown in Figure 3b or within the rotational limits of $[-15, 15]$ degrees. This mode, referred to as pose control, offers intuitive steering and high precision, making it ideal for object interaction tasks.

Control Mode 2 (Velocity Control): When the operator moves outside the boundaries of the EW, a haptic force/torque

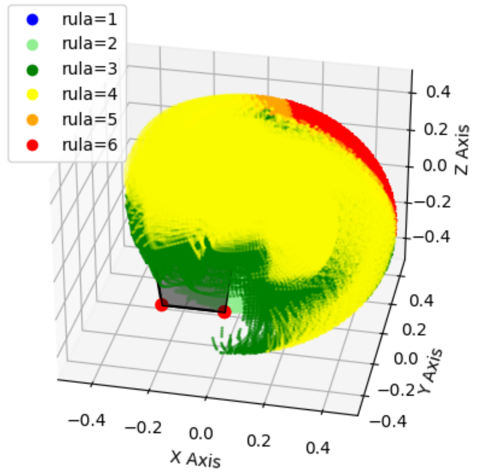

(a) Point cloud of all possible wrist positions, with each point representing a wrist position colored according to the corresponding RULA score for that arm configuration. Red points indicate wrist positions resulting from unergonomic arm configurations, while light green points represent positions from good ergonomic configurations. The blue points, hidden beneath the rest of the cloud, correspond to wrist positions from ergonomically excellent configurations (RULA=1), which are the target arm configurations in this study.

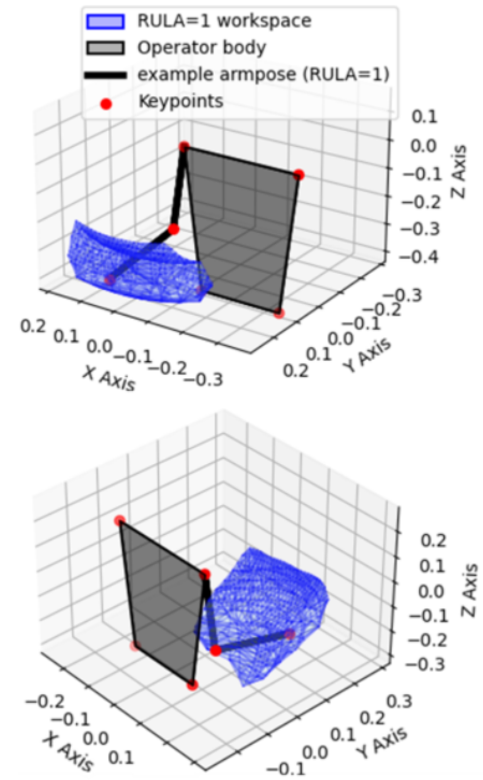

(b) The 3D body shown in blue is the Translational EW, derived from the arm configurations with RULA=1 scores in Figure 3a. The EW is presented from two different angles.

Fig. 3: EW based on wrist positions

is generated by the leader handle to guide the operator back towards the EW.

- In case of the **Translational EW**, this haptic force is calculated proportional to the smallest distance from the leader handle to the Translational EW. The larger the distance, the larger the haptic force guiding the operator back towards the EW.
- In case of the **Rotational EW**, the haptic torque is proportional to the error between the rotation of the leader handle and the rotational EW (-15° to 15° for each pitch, roll and yaw). The larger the error with respect to the ergonomic range, the larger the torque guiding the operator back towards the rotational EW.

See **Appendix B** for a more detailed description of how the haptic forces and torques are calculated.

The operator can resist the haptic forces to provide the follower robot with a translational and/or rotational velocity proportional to the force/torque exerted by the operator. Velocity control enables to dynamically reindex the follower's workspace, either by translation or rotation. By commanding a constant follower velocity while maintaining a fixed leader pose, the follower workspace is dynamically reindexed to a new location. For instance, to interact with a target object located outside the EW, the operator can first leverage velocity control, causing the follower to move while the leader remains stationary. This dynamically reindexes the follower's workspace toward the target, now enabling interaction with the object from within the EW boundaries using pose control.

C. Validation method

The proposed teleoperation system is evaluated through a teleoperation task performed using two control strategies: (1) a conventional pose-pose controller and (2) the proposed controller. This task is executed by an expert operator, who is required to guide the follower robot to two predefined target poses, see Figure 5. The operator remained seated, assuming no upper body movement or rotation. Following sequence had to be executed:

1) Translate follower towards Target A (without rotation).
2) Rotate follower so that follower frame aligns with Target A frame.
3) Translate follower towards Target B (without rotation).

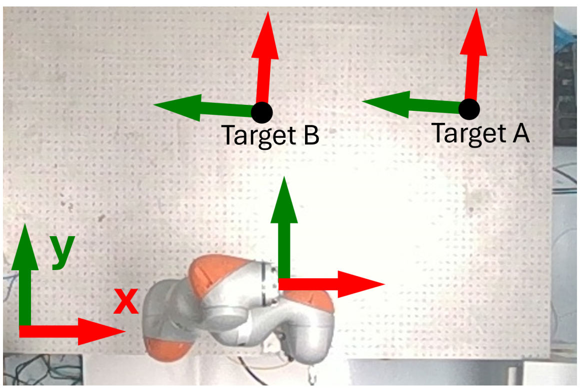

Fig. 5: Teleoperation task with target frames. Follower frame initially aligns with the global frame.

Initialize variables;
while *running* **do**
  Get leader pose: position $\mathbf{p}_{h,t}$, rotation $\mathbf{r}_{h,t}$;
  if $\mathbf{r}_{h,t}$ *is inside rotational EW* **then**
    Rotation control mode:
    Set torque feedback to zero: $\mathbf{t}_h = [0,0,0]$;
    Calculate offset: $\mathbf{r}_{offset,t} = \mathbf{r}_{ref,t-1} - \mathbf{r}_{h,t-1}$;
    Update follower rotation: $\mathbf{r}_{ref,t} = \mathbf{r}_{h,t} + \mathbf{r}_{offset,t}$;
  else
    Velocity control mode:
    Calculate torque feedback $\mathbf{t}_h$ based on distance from $\mathbf{r}_{h,t}$ to rotational EW;
    Set follower velocity: $\dot{\mathbf{r}}_{ref,t} = -scale * \mathbf{t}_h$;
    Calculate rotational increment:
    $\Delta\mathbf{r}_{ref,t} = \dot{\mathbf{r}}_{ref,t} * \Delta t$;
    Update follower rotation:
    $\mathbf{r}_{ref,t} = \mathbf{r}_{ref,t-1} + \Delta\mathbf{r}_{ref,t}$;
    Update offset: $\mathbf{r}_{offset,t} = \mathbf{r}_{offset,t-1} + \Delta\mathbf{r}_{ref,t}$;
  Calculate current rotation matrix $\mathbf{R}_t$ from $\mathbf{r}_{offset,t}$
  if $\mathbf{p}_{h,t}$ *is inside translational EW* **then**
    Position control mode:
    Set force feedback to zero: $\mathbf{f}_h = [0,0,0]$;
    Calculate positional increment:
    $\Delta\mathbf{p}_{h,t} = \mathbf{p}_{h,t} - \mathbf{p}_{h,t-1}$;
    Calculate rotated increment:
    $\Delta\mathbf{p}_{ref,t} = \mathbf{R}_t \cdot \Delta\mathbf{p}_{h,t}$;
    Update follower position:
    $\mathbf{p}_{ref,t} = \mathbf{p}_{h,t-1} + \Delta\mathbf{p}_{ref,t}$;
  else
    Velocity control mode:
    Calculate force feedback $\mathbf{f}_h$ based on distance from $\mathbf{p}_{h,t}$ to EW;
    Set follower velocity: $\dot{\mathbf{p}}_{ref,t} = -scale * \mathbf{f}_h$;
    Calculate positional increment:
    $\Delta\mathbf{p}_{incr,t} = \dot{\mathbf{p}}_{ref,t}\Delta t$;
    Calculate rotated increment:
    $\Delta\mathbf{p}_{ref,t} = \mathbf{R}_t \cdot \Delta\mathbf{p}_{incr,t}$;
    Update follower position:
    $\mathbf{p}_{ref,t} = \mathbf{p}_{ref,t-1} + \Delta\mathbf{p}_{ref,t}$;
  Send $\mathbf{t}_h$ and $\mathbf{f}_h$ to leader device;
  Send $\mathbf{p}_{ref,t}$ and $\mathbf{p}_{ref,t}$ to follower;
  Update previous poses:
  $\mathbf{p}_{h,t-1} = \mathbf{p}_{h,t}$;
  $\mathbf{p}_{ref,t-1} = \mathbf{p}_{ref,t}$;
  $\mathbf{r}_{h,t-1} = \mathbf{r}_{h,t}$;
  $\mathbf{r}_{ref,t-1} = \mathbf{r}_{ref,t}$;

Fig. 4: Pseudocode for sending reference pose (existing of $\mathbf{r}_{ref}$ and $\mathbf{p}_{ref}$) to the follower based on the leader pose $\mathbf{r}_h$ and $\mathbf{p}_h$. $\mathbf{R}_t$ is the rotation matrix corresponding to the three rotations $\mathbf{r}_{offset,t} = [pitch, roll, yaw]$

Throughout the task, the operator's posture is evaluated using the RULA method. Validation is performed by comparing the ergonomic scores from both control strategies. The primary focus is on periods of object interaction, which require enhanced operator ergonomics due to their extended duration.

Since the proposed controller operates entirely in 3D, the task is executed in 3D. However, Targets A and B share the same z-coordinate and only have a rotation about the global z-axis (yaw rotation). This setup is sufficient for a proof-of-concept of the controller and enhances clarity of the results, as the they can be displayed in 2D, ignoring z-translations and rotation about the x-axis (pitch) and y-axis (roll).

III. Results

A. Experimental setup

The proposed teleoperation system is demonstrated using a Sigma.7 haptic device [27] as the leader and a KUKA iiwa 14 robotic arm [50] as the follower. ROS is used as the communication framework The proposed controller sends its reference commands to an external controller that controls the KUKA 14 follower robot. This external controller consist of an impedance controller [51], build on top of the iiwa_ros package developed by EPFL [52]. The teleoperation system is unilateral. The only forces rendered on the leader side are the haptic forces generated during the velocity control mode (refer back to Section II-B). See **Appendix C** for more information on the ROS framework.

To quantify the operator's posture in real-time, movements are recorded using a RealSense D435 depth camera. This device captures both RGB and depth images. The RGB images are processed using the pose detection model MMPose [53], which identifies the 2D pixel coordinates of body keypoints, including the nose, shoulders, elbows, wrists, and hips. An example of an RGB and depth image pair with the corresponding keypoints is shown in Figure 6a. By combining the depth image with the camera intrinsics, the 3D positions of the 2D keypoints are calculated. Connecting the relevant 3D keypoints produces a virtual stick model of the human operator, as illustrated in Figure 6b. This virtual stick model serves as input for the RULA method to compute a real-time ergonomic score. Utilizing a depth camera is preferred over invasive techniques. such as IMUs [54] or motion capture systems with body markers [55, 56], as it eliminates the need for attaching instruments to the operator.

B. Workspace reindexing results

Figures 7 and 8 present spatial visualizations of the task execution using the proposed controller. To dynamically reindex the workspace towards Target A, the operator moved outside the translational EW between 2.99s and 12.50s. To align with the Target A frame, the operator then moved beyond the limits of the rotational EW, causing the workspace to rotate (this occurred between 18.10s and 25.12s, see Figure 9). To reach Target B, the operator subsequently moved the leader outside the translational EW in the y-direction between 25.73s and 40.05s, which resulted in the dynamic reindexing of the follower in the global x-direction due to the rotated follower workspace.

Since the Targets share the same z-value and only have a rotation about the z-axis (yaw), the primary variables of interest are the x- and y-coordinates along with the yaw rotation. Figure 9 shows these variables over time for the same task execution as presented in Figures 7 and 8. The periods where pose control is active are highlighted in light blue, whereas the periods of velocity control, enabling dynamic workspace indexing, are shown in white. During the periods [2.99s, 12.50s] and [30.73s, 43.05s], the follower workspace was being reindexed by controlling the translational velocity. When the leader leaves the translational workspace (EW), an error relative to the EW is introduced which subsequently generates a haptic force. Similarly, the follower's workspace was reindexed by controlling the rotational velocity during period [18.10s, 25.12s].

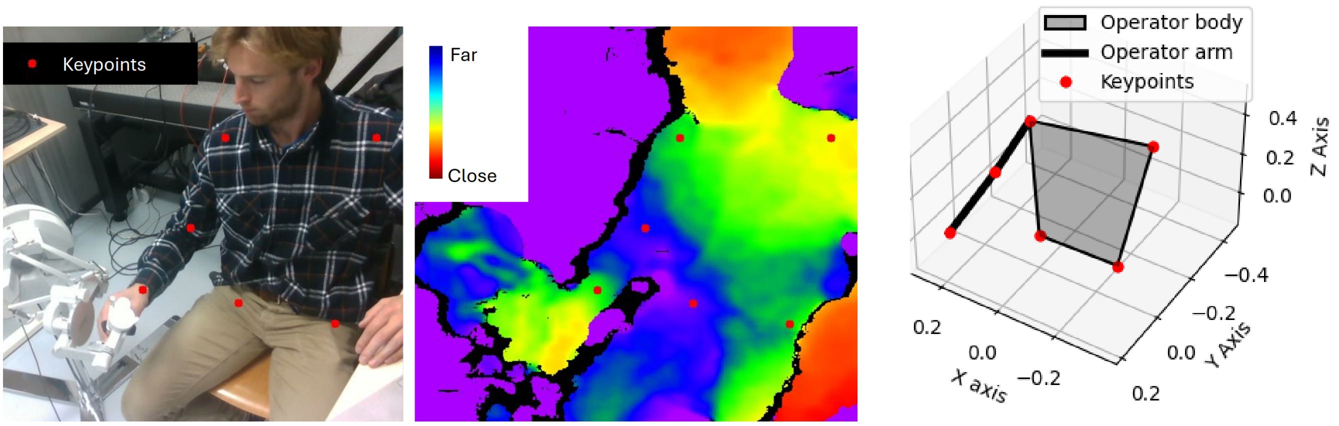

(a) RGB and depth image captured using the RealSense D435. Left: RGB image with body keypoints determined using pose estimation model MMPose [53]. Right: Corresponding depth image with overlay of the keypoints.

(b) 3D stick model obtained based on the data gathered by the RealSense camera.

Fig. 6: Data processing from RGB and depth image to a 3D stick model of the operator

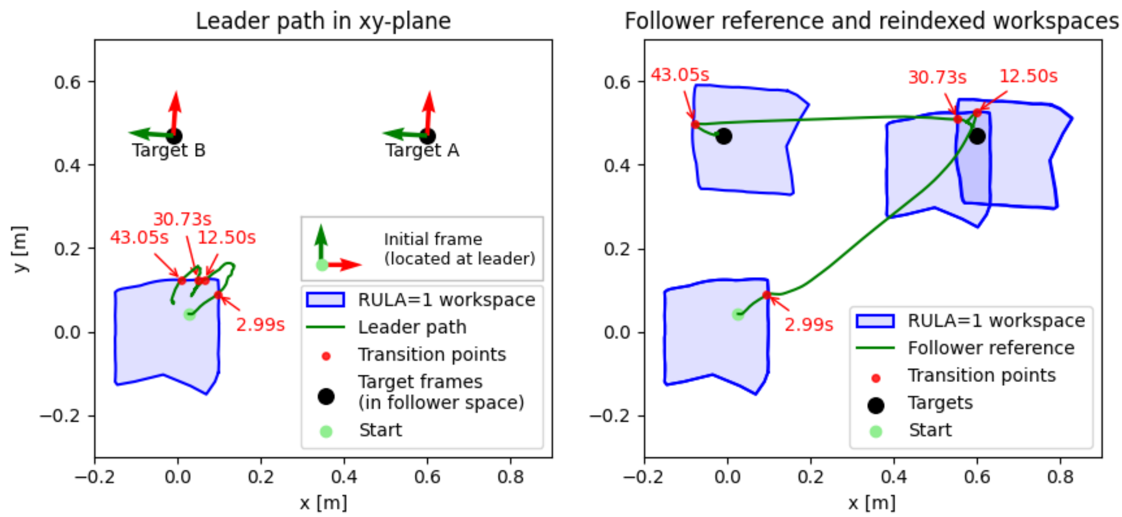

Fig. 7: Workspace reindexing results. Left: leader workspace and target frames, right: follower workspace with reindexed EW's over time. Note that the timestamps corresponding to rotational reindexing are not shown.

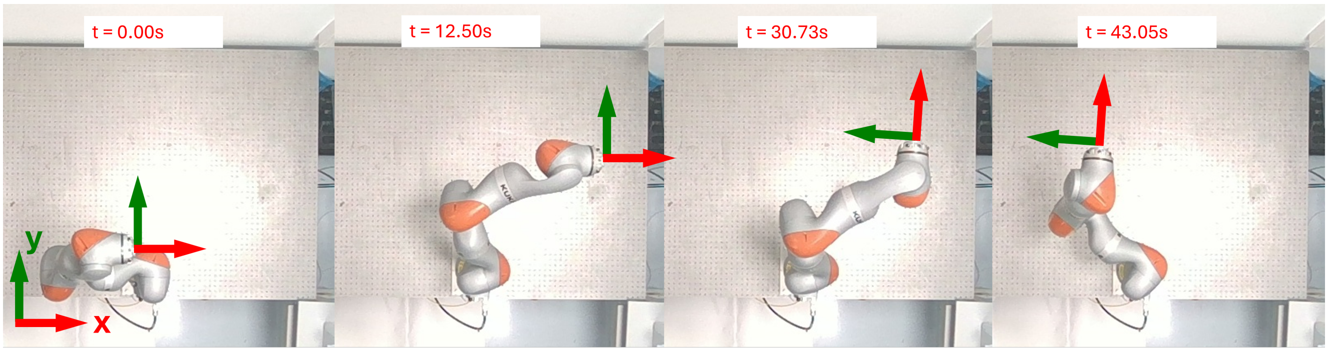

Fig. 8: Follower robot at timestamps corresponding to Figure 7

C. Ergonomic results

Figures 10a and 10b present the RULA scores for the task executed with both controllers. As RULA is a discrete metric with integer-based transitions, abrupt changes are present in the recorded RULA scores. A Gaussian filter is applied to enhance readability by smoothing the data. **Appendix D** presents the non-smoothed data and score graphs for individual RULA components (upper arm, lower arm, wrist), offering insights into RULA variations over time.

- $[2.99s, 12.50s]$: The operator leaves the translational EW to dynamically reindex the workspace using the proposed controller, increasing $\text{RULA}_{\text{prop}}$. Also $\text{RULA}_{\text{conv}}$ increases to 3 as the operator moves outside the EW. Around 10 seconds, $\text{RULA}_{\text{conv}}$ further increases to 4 as the operator extends their arm to reach Target A.
- $[12.50s, 18.10s]$: Operator moves back into translational EW for object interaction, therefore decreasing $\text{RULA}_{\text{prop}}$ back to 1. $\text{RULA}_{\text{conv}}$ remains at 4 as Target A is far outside the EW.
- $[18.10s, 25.12s]$: The operator leaves the rotational EW to reindex the workspace through rotation. As the wrist rotates, $\text{RULA}_{\text{prop}}$ increases to 2. $\text{RULA}_{\text{conv}}$ increases from 4 to 5 due to the added rotation towards the Target A frame.
- $[25.12s, 30.73s]$: The operator returns to the EW to interact with Target A, lowering $\text{RULA}_{\text{prop}}$ to 1. $\text{RULA}_{\text{conv}}$ remains at 5 as the operator's arm stays in the same configuration.
- $[30.73s, 43.05s]$: $\text{RULA}_{\text{prop}}$ sligthly increases as the operator translates outside the EW. The discrete nature of the RULA rules causes $\text{RULA}_{\text{prop}}$ to fluctuate near the threshold boundaries. As a result of the Gaussian filter, the scores become non discrete. $\text{RULA}_{\text{conv}}$ decreases to 4 as the operator moves their arm from the side towards the midline.
- $[43.05s, 60.0s]$: The operator returns to the EW to interact with Target B, reducing $\text{RULA}_{\text{prop}}$ to 1. $\text{RULA}_{\text{conv}}$ remains at 4 as the operator interacts with Target B.

The proposed controller consistently maintains lower RULA values throughout the teleoperation task. Dynamic workspace reindexing allows the operator to perform object interaction while maintaining a RULA score of 1.

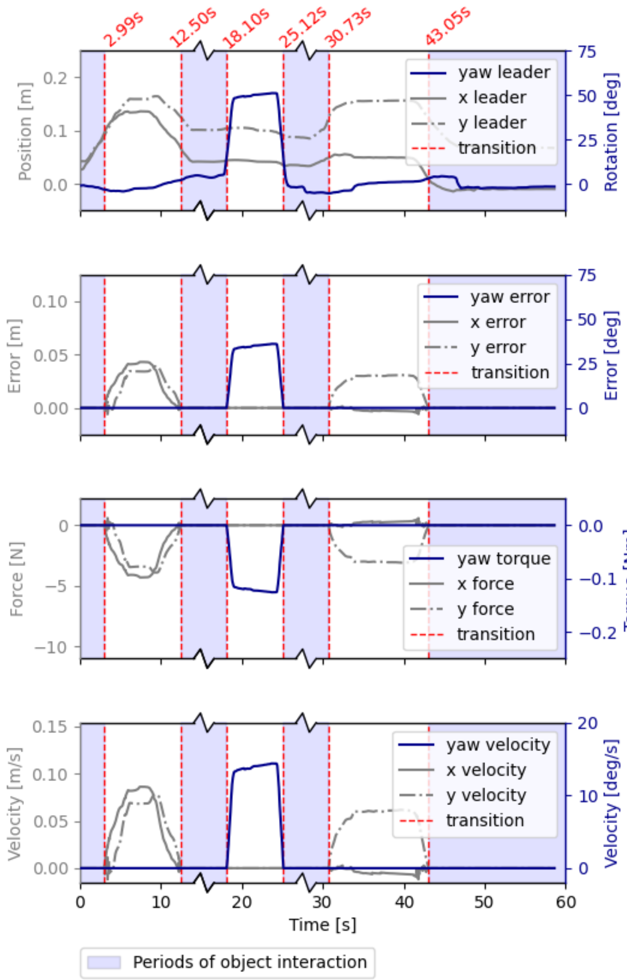

Fig. 9: Task data using the proposed controller. Plot 1) Leader pose. Plot 2) Error from leader to EW. Plot 3) Haptic force on leader handle. Plot 4) Reference velocity for follower. The zigzag lines along the top and bottom plot borders represent intervals between dynamic reindexing. These periods are of particular interest as they correspond to object interaction activities, which may last for an extended duration. Therefor, it is essential to ensure the operator maintains an ergonomic posture during these intervals.

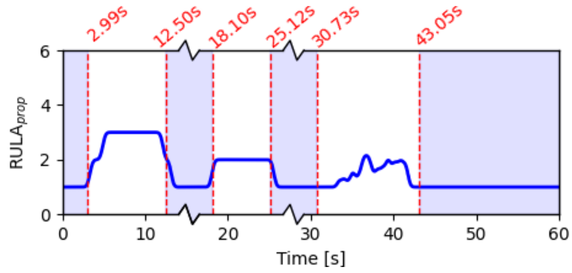

(a) RULA score (RULA$_{\mathrm{prop}}$) during execution of the task using the proposed controller

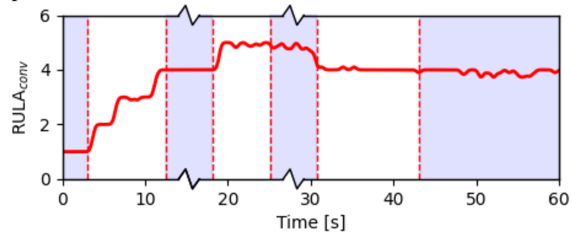

(b) RULA score (RULA$_{\mathrm{conv}}$) during execution of the task using the conventional controller

Fig. 10: RULA scores during both task executions. The proposed controller reduced the RULA score to its most ergonomic value during object interaction. In contrast, the conventional controller required the operator to extend their arm to reach objects, resulting in higher RULA scores.

IV. DISCUSSION

The primary advantage of the proposed controller is its ability to enhance ergonomics in teleoperation. By dynamically reindexing the workspace toward target objects, it is ensured that object interactions are consistently performed from an ergonomic posture. Furthermore, dynamic reindexing successfully addresses workspace limitations without requiring clutching or scaling. Between reindexing periods, pose control facilitates intuitive interaction with target objects.

A limitation of the system is that it is mainly effective when prolonged interactions with target objects are required. Figures 9 and 10 highlight the periods of object interaction. When these interactions are brief, the operator remains in a non-ergonomic position for only a short duration, making the benefits of ergonomic optimization less significant. Furthermore, Figure 8 demonstrates that reindexing from one target to another requires a significant amount of time. If the object interaction periods are short, a relatively large portion of the task would be spent on workspace reindexing, reducing the time efficiency of the controller.

Another limitation of the controller is the shape of the EW. The EW is entirely derived from the rules of the RULA method, without consideration for intuitive human interaction. While this approach promotes ergonomic posture for the operator, it may not always align with the operator's natural movements. Furthermore, the 3D shape of the EW may reduce the predictability of transitions between pose control and velocity control. Effective use of the system requires the operator to become familiar with the EW's shape to anticipate control mode transitions.

For this research, RULA was adapted using certain simplifications. The complete RULA method includes rules regarding the operator upper body as well, whereas this research only focuses on the arm-related rules. It was assumed that there was no upper body movement or rotation during task execution. Since the task was performed while seated in a chair, the operator's upper body remained relatively still, resulting in no significant change in the RULA score due to upper body movement. Additionally, some simplifications were made to the RULA method concerning the operator's arm. The boundaries of the EW are determined by wrist positions. However, the operator holds the leader handle with their hand rather than their wrist, introducing a difference of $p_{wrist} - p_{handpalm}$. This difference is compromised by translating the EW towards the operator. However, this holds true only if the operator's lower arm is perfectly aligned with the y-axis (as in Figure 3b). Since the lower arm is often rotated, this translation is an approximation. Furthermore, the operator wrist rotation is determined by directly taking the handle rotation ($\theta_{wrist} = \theta_{handle}$). However, the operator can rotate the handle independently of the wrist, as elbow movement rotates the handle while the wrist maintains a constant rotation.

V. Future Works

As discussed in Section IV, this research adapted RULA with certain simplifications. Future research could enhance the proposed controller by incorporating ergonomic guidelines for the upper body and refining the current approach for the arm, rather than relying on current simplifications.

Reindexing the rotation of the follower workspace creates an offset between the leader and follower, adding additional difficulty in teleoperation. No measures have been implemented yet to address this issue. A camera could be mounted on the end effector of the follower to provide a first-person view, thereby overcoming the issues with a rotational offset.

Section IV highlights that workspace reindexing requires a significant amount of time. This issue can be mitigated by increasing the scaling factor, which would increase the velocity of workspace reindexing. Future research could focus on refining this scaling factor to increase reindexing speed while preserving teleoperation accuracy.

References

[1] World robotics report: "all-time high" with half a million robots installed in one year, 10 2022.

[2] Michal Bartoš, Vladimír Bulej, Martin Bohušík, Ján Stanček, Vitalii Ivanov, and Peter Macek. An overview of robot applications in automotive industry. *Transportation Research Procedia*, 55:837–844, 2021. 14th International scientific conference on sustainable, modern and safe transport.

[3] Liyana Wijayathunga, Alexander Rassau, and Douglas Chai. Challenges and solutions for autonomous ground robot scene understanding and navigation in unstructured outdoor environments: A review. *Applied Sciences*, 13(17), 2023.

[4] Rajni V. Patel, S. Farokh Atashzar, and Mahdi Tavakoli. Haptic feedback and force-based teleoperation in surgical robotics. *Proceedings of the IEEE*, 110(7):1012–1027, 2022.

[5] Vitalii Pruks, Kwang-Hyun Lee, and Jee-Hwan Ryu. Shared teleoperation for nuclear plant robotics using interactive virtual guidance generation and shared autonomy approaches. In *2018 15th International Conference on Ubiquitous Robots (UR)*, pages 91–95, 2018.

[6] Udaka Manawadu, Hiroaki Ogawa, Keito Shishiki, Yuki Funayama, Hiroto Sasaki, Takuma Suzuki, and Keitaro Naruse. Towards developing a teleoperation system for a disaster response robot. *SHS Web of Conferences*, 102:04005, 01 2021.

[7] Boston Dynamics. Spot® - the agile mobile robot. https://bostondynamics.com/products/spot/. Accessed: 2025-01-24.

[8] Boston Dynamics. Spot to the rescue. https://bostondynamics.com/blog/spot-to-the-rescue/. Accessed: 2025-01-23.

[9] Bernhard Haist. Setting up and managing a remote maintenance operation for fusion. *Fusion Engineering and Design*, 83(10):1841–1844, 2008. Proceedings of the Eight International Symposium of Fusion Nuclear Technology.

[10] K.A. Manocha, N. Pernalete, and R.V. Dubey. Variable position mapping based assistance in teleoperation for nuclear cleanup. In *Proceedings 2001 ICRA. IEEE International Conference on Robotics and Automation (Cat. No.01CH37164)*, volume 1, pages 374–379 vol.1, 2001.

[11] Christian Hatzfeld, Carsten Neupert, Sebastian Matich, Manuel Braun, Johannes Bilz, Jonas Johannink, Johanna Miller, Peter P. Pott, Helmut F. Schlaak, Mario Kupnik, Roland Werthschützky, and Andreas Kirschniak. A teleoperated platform for transanal single-port surgery: Ergonomics and workspace aspects. In *2017 IEEE World Haptics Conference (WHC)*, pages 1–6, 2017.

[12] Intuitive. Intuitive da vinci. https://www.intuitive.com/en-us/products-and-services/da-vinci. Accessed: 2025-01-24.

[13] B. Hannaford, L. Wood, D.A. McAffee, and H. Zak. Performance evaluation of a six-axis generalized force-reflecting teleoperator. *IEEE Transactions on Systems, Man, and Cybernetics*, 21(3):620–633, 1991.

[14] T.B. Sheridan. Telerobotics. *Automatica*, 25(4):487–507, 1989.

[15] Henri Boessenkool, David A. Abbink, Cock J.M. Heemskerk, and Frans C.T. van der Helm. Haptic shared control improves tele-operated task performance towards performance in direct control. In *2011 IEEE World Haptics Conference*, pages 433–438, 2011.

[16] Henri Boessenkool, David A. Abbink, Cock J.M. Heemskerk, Frans C.T. van der Helm, and Jeroen G.W. Wildenbeest. A task-specific analysis of the benefit of haptic shared control during telemanipulation. *IEEE Transactions on Haptics*, 6(1):2–12, 2013.

[17] Peter F. Hokayem and Mark W. Spong. Bilateral teleoperation: An historical survey. *Automatica*, 42(12):2035–2057, 2006.

[18] Kamil Kukliński, Kerstin Fischer, Ilka Marhenke, Franziska Kirstein, Maria V. aus der Wieschen, Dorthe Sølvason, Norbert Krüger, and Thiusius Rajeeth Savarimuthu. Teleoperation for learning by demonstration: Data glove versus object manipulation for intuitive robot control. In *2014 6th International Congress on Ultra Modern Telecommunications and Control Systems and Workshops (ICUMT)*, pages 346–351, 2014.

[19] Shuo Zhu, Angus Stuttaford-Fowler, Ashraf Fahmy, Chunxu Li, and Johann Sienz. Development of a low-cost data glove using flex sensors for the robot hand teleoperation. In *2021 3rd International Symposium on Robotics Intelligent Manufacturing Technology (ISRIMT)*, pages 47–51, 2021.

[20] E. Sanchez, A. Rubio, and A. Avello. An intuitive force

feed-back to avoid singularity proximity and workspace boundaries in bilateral controlled systems based on virtual springs. In *IEEE/RSJ International Conference on Intelligent Robots and Systems*, volume 2, pages 1302–1307 vol.2, 2002.

[21] P. Chotiprayanakul and D.K. Liu. Workspace mapping and force control for small haptic device based robot teleoperation. In *2009 International Conference on Information and Automation*, pages 1613–1618, 2009.

[22] F. Conti and O. Khatib. Spanning large workspaces using small haptic devices. In *First Joint Eurohaptics Conference and Symposium on Haptic Interfaces for Virtual Environment and Teleoperator Systems. World Haptics Conference*, pages 183–188, 2005.

[23] A Fischer and Judy Vance. Phantom haptic device implemented in a projection screen virtual environment. pages 225–229, 05 2003.

[24] Lawrence H. Kim, Clifford Bargar, Yuhang Che, and Allison M. Okamura. Effects of master-slave tool misalignment in a teleoperated surgical robot. In *2015 IEEE International Conference on Robotics and Automation (ICRA)*, pages 5364–5370, 2015.

[25] Shen Treratanakulchai and Ferdinando Rodriguez y Baena. A passive decoupling mechanism for misalignment compensation in master-slave teleoperation. *IEEE Transactions on Medical Robotics and Bionics*, 3(1):285–288, 2021.

[26] Jessie Y. C. Chen, Ellen C. Haas, and Michael J. Barnes. Human performance issues and user interface design for teleoperated robots. *IEEE Transactions on Systems, Man, and Cybernetics, Part C (Applications and Reviews)*, 37(6):1231–1245, 2007.

[27] Force Dimension. https://www.forcedimension.com/products/sigma. Accessed: 2024-11-15.

[28] Haption. https://www.haption.com/product/virtuose6d. Accessed: 2025-01-07.

[29] Guanyang Liu, Xuda Geng, Lingzhi Liu, and Yan Wang. Haptic based teleoperation with master-slave motion mapping and haptic rendering for space exploration. *Chinese Journal of Aeronautics*, 32(3):723–736, 2019.

[30] L. Dominjon, A. Lecuyer, J.-M. Burkhardt, G. Andrade-Barroso, and S. Richir. The ”bubble” technique: interacting with large virtual environments using haptic devices with limited workspace. In *First Joint Eurohaptics Conference and Symposium on Haptic Interfaces for Virtual Environment and Teleoperator Systems. World Haptics Conference*, pages 639–640, 2005.

[31] Chiedu N. Mokogwu and Keyvan Hashtrudi-Zaad. A hybrid position–rate teleoperation system. *Robotics and Autonomous Systems*, 141:103781, 2021.

[32] Zhiguo Lv, Yan Li, and Hangen He. An optimization-based arm posture prediction in presence of obstacles. In *2008 9th International Conference on Computer-Aided Industrial Design and Conceptual Design*, pages 193–197, 2008.

[33] Roger M Enoka and Jacques Duchateau. Muscle fatigue: what, why and how it influences muscle function. *The Journal of physiology*, 586(1):11–23, 2008.

[34] Álvaro Gil Andrés, Niek Beckers, David A. Abbink, and Luka Peternel. Arbitration of authority in physical human-robot collaboration with combined preventive and reactive fatigue management. In *2022 9th IEEE RAS/EMBS International Conference for Biomedical Robotics and Biomechatronics (BioRob)*, pages 1–6, 2022.

[35] Rok Goljat, Jan Babič, Tadej Petrič, Luka Peternel, and Jun Morimoto. Power-augmentation control approach for arm exoskeleton based on human muscular manipulability. In *2017 IEEE International Conference on Robotics and Automation (ICRA)*, pages 5929–5934, 2017.

[36] Soheil Gholami, Francesco Tassi, Elena De Momi, and Arash Ajoudani. A reconfigurable interface for ergonomic and dynamic tele-locomanipulation. In *2021 IEEE/RSJ International Conference on Intelligent Robots and Systems (IROS)*, pages 4260–4267, 2021.

[37] Soheil Gholami, Marta Lorenzini, Elena De Momi, and Arash Ajoudani. Quantitative physical ergonomics assessment of teleoperation interfaces. *IEEE Transactions on Human-Machine Systems*, 52(2):169–180, 2022.

[38] Luka Peternel, Tadej Petrič, and Jan Babič. Robotic assembly solution by human-in-the-loop teaching method based on real-time stiffness modulation. *Autonomous Robots*, 42:1–17, 2018.

[39] Clemente Lauretti, Francesca Cordella, Christian Tamantini, Cosimo Gentile, Francesco Scotto di Luzio, and Loredana Zollo. A surgeon-robot shared control for ergonomic pedicle screw fixation. *IEEE Robotics and Automation Letters*, 5(2):2554–2561, 2020.

[40] Baptiste Busch, Guilherme Maeda, Yoan Mollard, Marie Demangeat, and Manuel Lopes. Postural optimization for an ergonomic human-robot interaction. In *2017 IEEE/RSJ International Conference on Intelligent Robots and Systems (IROS)*, pages 2778–2785, 2017.

[41] Rahaf Rahal, Giulia Matarese, Marco Gabiccini, Alessio Artoni, Domenico Prattichizzo, Paolo Robuffo Giordano, and Claudio Pacchierotti. Caring about the human operator: Haptic shared control for enhanced user comfort in robotic telemanipulation. *IEEE Transactions on Haptics*, 13(1):197–203, 2020.

[42] Sue Hignett and Lynn Mcatamney. Rapid entire body assessment (reba). *Applied ergonomics*, 31:201–5, 05 2000.

[43] L Mcatamney and E. N. Corlett. Rula: a survey method for the investigation of work-related upper limb disorders. *Applied ergonomics*, 24 2:91–9, 1993.

[44] Luka Peternel, Cheng Fang, Marco Laghi, Antonio Bicchi, Nikos Tsagarakis, and Arash Ajoudani. Human arm posture optimisation in bilateral teleoperation through interface reconfiguration. In *2020 8th IEEE RAS/EMBS International Conference for Biomedical Robotics and Biomechatronics (BioRob)*, pages 1102–1108, 2020.

[45] Rahid Zaman, Yujiang Xiang, Ritwik Rakshit, and James Yang. Hybrid predictive model for lifting by integrating skeletal motion prediction with an opensim musculoskeletal model. *IEEE Transactions on Biomedical Engineering*, 69(3):1111–1122, 2022.

[46] Marta Lorenzini, Wansoo Kim, and Arash Ajoudani. An online multi-index approach to human ergonomics assessment in the workplace. *IEEE Transactions on Human-Machine Systems*, 52(5):812–823, 2022.

[47] N. Tsagarakis, D.G. Caldwell, and G.A. Medrano-Cerda. A 7 dof pneumatic muscle actuator (pma) powered exoskeleton. In *8th IEEE International Workshop on Robot and Human Interaction. RO-MAN '99 (Cat. No.99TH8483)*, pages 327–333, 1999.

[48] Cheng Fang, Luka Peternel, Wansoo Kim, Arash Ajoudani, and Henrik Petersen. An intuitive binary work-condition map for interactive learning of ergonomic arm postures, 11 2019.

[49] J. Rosen, J.C. Perry, N. Manning, S. Burns, and B. Hannaford. The human arm kinematics and dynamics during daily activities - toward a 7 dof upper limb powered exoskeleton. In *ICAR '05. Proceedings., 12th International Conference on Advanced Robotics, 2005.*, pages 532–539, 2005.

[50] KUKA AG. https://my.kuka.com/s/product/lbr-iiwa-14-r820. Accessed: 2025-16-01.

[51] Nicky Mol. iiwa_impedance_control. https://gitlab.tudelft.nl/nickymol/iiwa_impedance_control. Accessed: 2025-01-16.

[52] Konstantinos Chatzilygeroudis, Matthias Mayr, Bernardo Fichera, and Aude Billard. iiwa_ros: A ros stack for kuka's iiwa robots using the fast research interface, 2019.

[53] MMPose Contributors. Openmmlab pose estimation toolbox and benchmark. https://github.com/open-mmlab/mmpose, 2020.

[54] Justus Brosche, Hannes Wackerle, Peter Augat, and Hermann Lödding. Individualized workplace ergonomics using motion capture. *Applied Ergonomics*, 114:104140, 2024.

[55] Yahui Bai, Huimin Hu, Yinxia Li, Chaoyi Zhao, Ling Luo, and Rui Wang. Research methods for human activity space based on vicon motion capture system. In *2017 5th International Conference on Enterprise Systems (ES)*, pages 202–206, 2017.

[56] M. Gregor, Petr Horejsi, and Šimon Michal. Case study: Motion capture for ergonomics. pages 468–476, 01 2015.

Appendix A

RULA Adaptation

The Rapid Upper Limb Assessment (RULA) provides guidelines for quantifying the ergonomic quality of a person's posture. Figure A.1 illustrates the RULA rules considered in this project. While RULA includes additional criteria, only the arm-related rules are used for simplicity. From these arm-related rules, only the body geometry dependent rules are taken into account. There are two other arm-related rules that take into account (1) repetitive arm movements and (2) force on the operator arm. Repetitive arm movements are a function of time, and therefore complicate the real-time calculation of the RULA score. For that reason, this rule is omitted in the RULA score. Furthermore, arm force is left out as the forces from the haptic device are always smaller than the force that would be penalized by RULA.

A.1. Wrist score

According to Step 3 and Step 4 of the RULA sheet, wrist rotations are penalized with higher scores. Since measuring wirst rotation using the Realsense camera was too inaccurate, the wrist rotation was directly based on the rotation of the leader handle. Following rules are adapted from RULA:

Wrist Score: Because a rotation of 0 degrees does not really exist, a wrist yaw rotation within $[-5, 5]$ is assigned to a Wrist Score of 1. Outside this range and within $[-15, 15]$ is a Wrist score of 2. Otherwise a Wrist Score of 3 is assigned.

Wrist Twist: If the wrist roll angle is within $[-15, 15]$ degrees, Wrist Twist is given 1. If wrist roll is outside this range, Wrist Twist is 2.

Based on the scores for **Wrist Score** and **Wrist Twist**, a score is chosen from the columns in Figure A.1.

A.2. Arm score

According to RULA step 1 and 2, following rules are taken into account to penalize unergonomic arm configurations:

Shoulder pitch
The shoulder pitch angle is calculated with elbow y and z coordinates: $\theta_{\text{pitch}} = \arctan 2(x_{\text{elbow}}, -z_{\text{elbow}})$.
Angles are divided into different ranges to assign RULA scores:
- For angles between -20° and 20°, RULA = 1.
- For angles less than -20°, the RULA = 2.
- For angles between 20° and 45°, RULA = 2.
- For angles between 45° and 90°, RULA = is 3.
- For angles greater than 90°, RULA = 4.

Shoulder abduction
The shoulder abduction angle is calculated using the elbow x and z coordinates: $\theta_{\text{abduction}} = \tan^{-1}(x_{\text{elbow}}, -z_{\text{elbow}})$
If the shoulder abduction is less than 20°, the RULA score is 0; otherwise, it is 1.

Lower arm If the lower arm is positioned too far across midline or out to side of the body, +1 should be added to RULA score. Following condition is used to assess the position of the lower arm:
If the wrist position x coordinate is outside of the range $[-0.15, 0.10]$, +1 is added to RULA score.

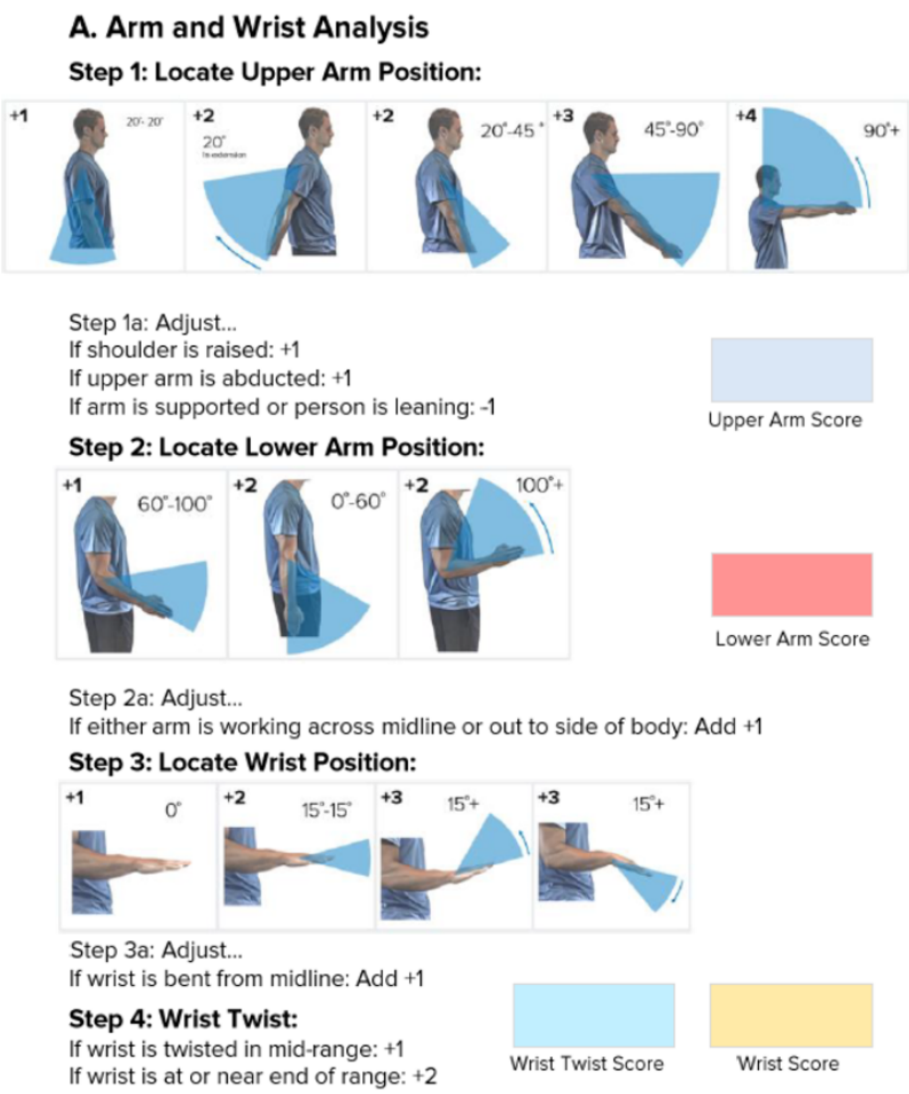

Scores

Table A		Wrist Score							
		1		2		3		4	
Upper Arm	Lower Arm	Wrist Twist		Wrist Twist		Wrist Twist		Wrist Twist	
		1	2	1	2	1	2	1	2
1	1	1	2	2	2	2	3	3	3
	2	2	2	2	2	3	3	3	3
	3	2	3	3	3	3	3	4	4
2	1	2	3	3	3	3	4	4	4
	2	3	3	3	3	3	4	4	4
	3	3	4	4	4	4	4	5	5
3	1	3	3	4	4	4	4	5	5
	2	3	4	4	4	4	4	5	5
	3	4	4	4	4	4	5	5	5
4	1	4	4	4	4	4	5	5	5
	2	4	4	4	4	4	5	5	5
	3	4	4	4	5	5	5	6	6
5	1	5	5	5	5	5	6	6	7
	2	5	6	6	6	6	7	7	7
	3	6	6	6	7	7	7	7	8
6	1	7	7	7	7	7	8	8	9
	2	8	8	8	8	8	9	9	9
	3	9	9	9	9	9	9	9	9

Figure A.1: RULA sheet

Elbow Bending The elbow bending angle θ_{elbow} is calculated in the plane that contains the points $\mathbf{x}_{\text{shoulder}}$, $\mathbf{x}_{\text{elbow}}$ $\mathbf{x}_{\text{wrist}}$. If the elbow bending angle is between 60° and 100°, RULA is 1; otherwise, it is 2.

Final RULA Scores: The upper arm RULA score is the sum of the **shoulder pitch** RULA score and the **shoulder abduction** RULA score. The lower arm RULA score is the sum of the **elbow bending** RULA score and the **lower arm** RULA score. The final RULA score is then determined from the table shown in Figure A.1.

A.3. Translational EW quantification

In order to define an Ergonomic Workspace (EW), all possible shoulder- and elbow rotations are iterated over to determine their corresponding wrist location. A RULA score is calculated for each individual arm configuration. The iteration process is based on the the authors arm sizes:

- L_{upperarm}: 30 cm
- L_{forearm}: 29 cm

By iterating over all possible arm configurations and calculating the corresponding RULA score, we obtain a RULA score per possible arm configuration (see sections A.3.1 and A.3.2 for elaboration on how arm configurations are modelled). Figure A.2 shows the all wrist positions colored according to the RULA score of the arm configuration resulting in that specific wrist position. The wrist positions clouds per RULA score are visualized in Figure A.3. Since this project is aiming for ergonomic teleoperation, the RULA = 1 workspace is used in the teleoperation system. This workspace is called the Ergonomic Workspace (EW).

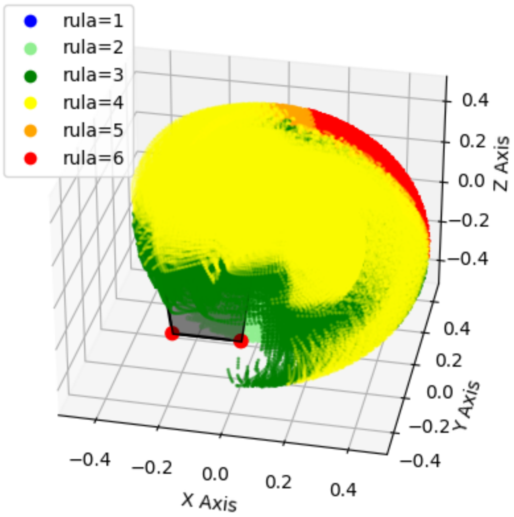

Figure A.2: RULA scores per arm configuration. Every single arm configuration contains a wrist position. This wrist position is shown with a dot colored according to the RULA score of the corresponding arm configuration.

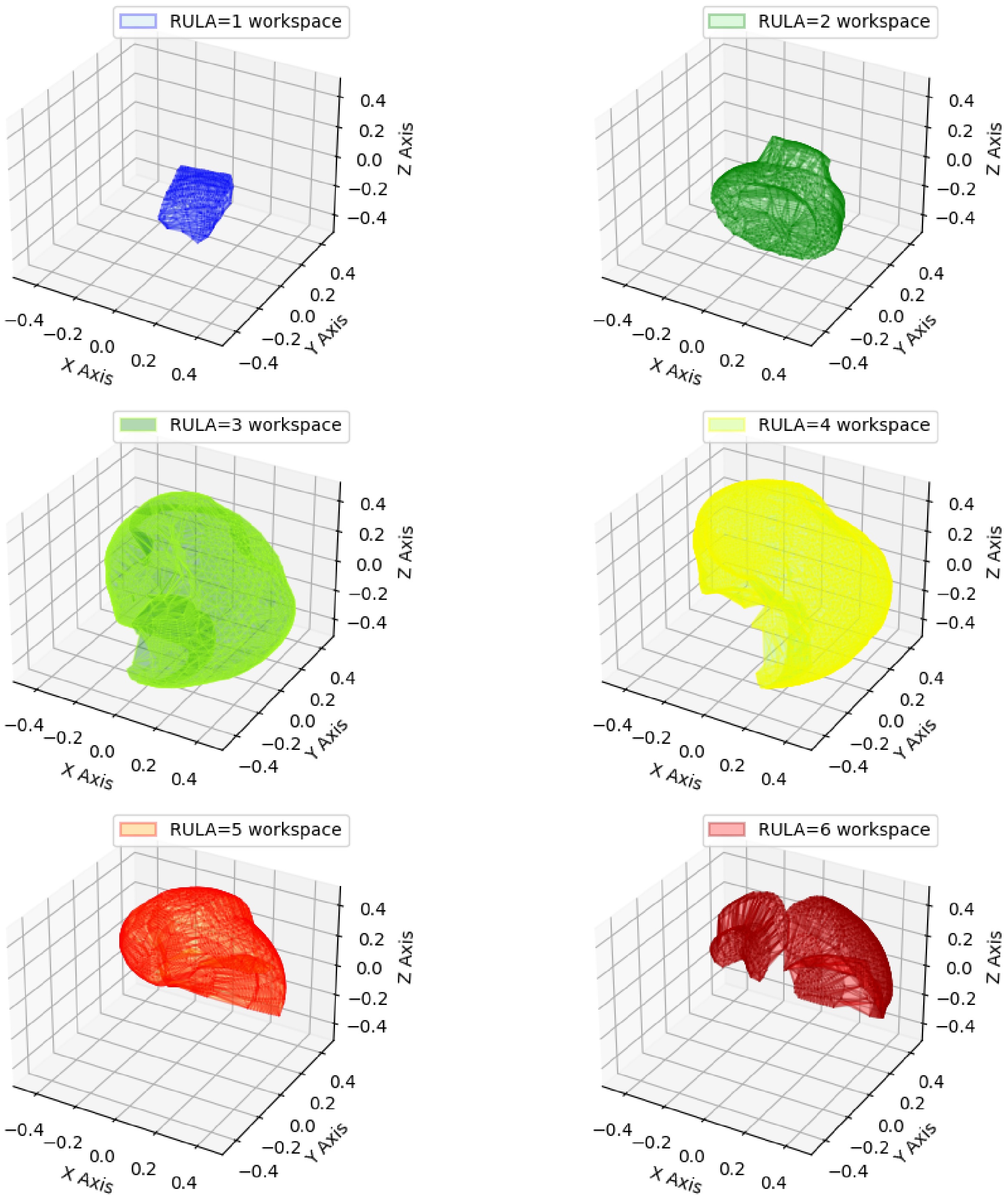

Figure A.3: Workspaces according to their RULA score

A.3.1. Elbow positions

By modeling the shoulder as a ball rotating in three directions, all possible elbow locations lay at a sphere with radius $= L_{\text{upperarm}}$ around the shoulder, see Figure A.4. To neglect upper arm rotations that are not possible, following filter is used:

$$\text{filter} = ((y > -x) \text{ and } (z < 0)) \text{ or } (((x > 0) \text{ or } (y > -x)) \text{ and } (z > 0)) \text{ and } (y >= -0.2) \quad \text{(eq A.1)}$$

Where the shoulder is located at $x, y, z = [0, 0, 0]$.

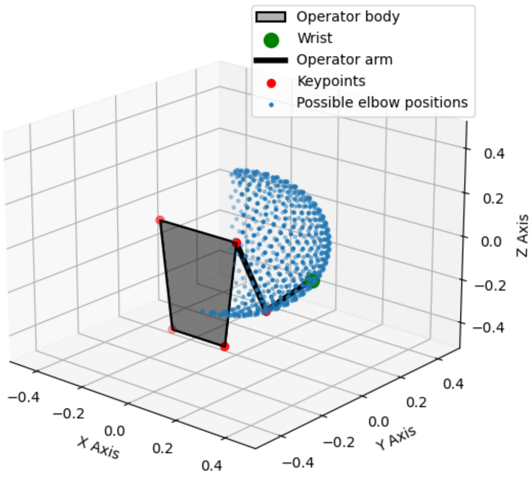

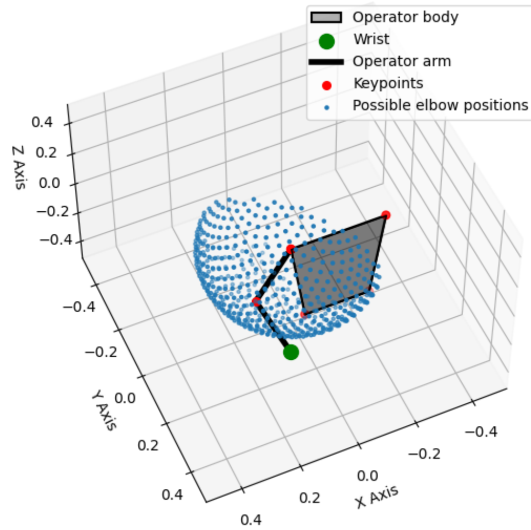

Figure A.4: All elbows points that are iterated over. The elbow points are subject to the filter defined in Equation eq A.1

A.3.2. Wrist positions

The wrist position depends on the elbow position, elbow bending angle, upper arm rotation and forearm length, see Figure A.5.

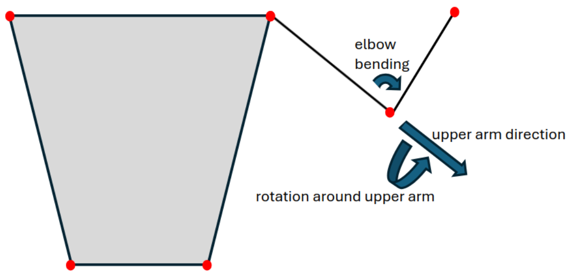

Figure A.5: Arm angle defenitions to calculate the wrist position

The normal to the plane defined by the elbow position, shoulder position, and the z-axis (used to rotate around the upper arm) is computed as:

$$\mathbf{n} = \frac{\mathbf{v_1} \times \mathbf{v_2}}{|\mathbf{v_1} \times \mathbf{v_2}|}$$

where:

$\mathbf{v_1} = \mathbf{x}_{\text{elbow}} - \mathbf{x}_{\text{shoulder}}$
$\mathbf{v_2} = \mathbf{z}_{\text{axis}} - \mathbf{x}_{\text{shoulder}}$

The upper arm direction $\mathbf{u}$ and the in-plane direction for elbow bending $\mathbf{v}$ are calculated:

$$\mathbf{u} = \frac{\mathbf{v_1}}{|\mathbf{v_1}|}, \quad \mathbf{v} = \frac{\mathbf{n} \times \mathbf{u}}{|\mathbf{n} \times \mathbf{u}|}$$

For a given elbow bending angle θ_{elbow}, the wrist position is computed as:

$$\mathbf{x}_{\text{wrist}} = \mathbf{x}_{\text{elbow}} + \mathbf{L}_{\text{forearm}} \left(\cos(\theta)\mathbf{u} + \sin(\theta)\mathbf{v} \right)$$

For each upper arm rotation angle ϕ, the rotation matrix $\mathbf{R}$ is calculated as:

$$R = \begin{bmatrix} \cos(\phi) + u_1^2(1-\cos(\phi)) & u_1u_2(1-\cos(\phi)) - u_3\sin(\phi) & u_1u_3(1-\cos(\phi)) + u_2\sin(\phi) \\ u_2u_1(1-\cos(\phi)) + u_3\sin(\phi) & \cos(\phi) + u_2^2(1-\cos(\phi)) & u_2u_3(1-\cos(\phi)) - u_1\sin(\phi) \\ u_3u_1(1-\cos(\phi)) - u_2\sin(\phi) & u_3u_2(1-\cos(\phi)) + u_1\sin(\phi) & \cos(\phi) + u_3^2(1-\cos(\phi)) \end{bmatrix}$$

Finally, the wrist position is rotated around the upper arm using the rotation matrix $\mathbf{R}$:

$$\mathbf{x}_{\text{wrist,rotated}} = \mathbf{x}_{\text{shoulder}} + R \left(\mathbf{x}_{\text{wrist}} - \mathbf{x}_{\text{shoulder}} \right)$$

Appendix B

Haptic force/torque feedback

B.1. Haptic force calculation

To compute the haptic force guiding the operator back into the EW, the current leader handle location $\mathbf{p} = (r_x, r_y, r_z)$ is evaluated against the EW (see **Appendix A**)

- If $\mathbf{p}$ is inside EW, the force is set to zero.
- If $\mathbf{p}$ is outside, the closest point on the EW surface is determined by iterating over its triangular facets (see Section B.3.
- The closest distance vector $\mathbf{d} = (d_x, d_y, d_z)$ is computed as:

$$\mathbf{d} = \mathbf{p}_{\text{closest}} - \mathbf{p} \qquad \text{(eq B.1)}$$

- The haptic force $\mathbf{f} = (f_x, f_y, f_z)$ is then computed as:

$$f_x = 100d_x, \quad f_y = 100d_y, \quad f_z = 100d_z \qquad \text{(eq B.2)}$$

  The scaling factor of 100 is chosen based on a trial with the haptic device so that the haptic force is just felt when the operator is on the boundary of the EW.

B.2. Haptic torque Calculation

The rotational haptic force is computed based on positional constraints within a predefined range $[r_{\min}, r_{\max}] = [-15, 15]$:

- If the rotational position r_x, r_y, r_z is outside this range, a corrective torque is applied, :

$$t_x = t_{\text{scale}}(r_{\min} - r_x), \quad \text{if } r_x < r_{\min} \text{ or } r_x > r_{\max} \qquad \text{(eq B.3)}$$
$$t_y = t_{\text{scale}}(r_{\min} - r_y), \quad \text{if } r_y < r_{\min} \text{ or } r_y > r_{\max} \qquad \text{(eq B.4)}$$
$$t_z = t_{\text{scale}}(r_{\min} - r_z), \quad \text{if } r_z < r_{\min} \text{ or } r_z > r_{\max} \qquad \text{(eq B.5)}$$

- Otherwise, the torque is set to zero.

B.3. Distance to EW

A C++ node is used to calculate the distance to the EW in real-time. The EW points are imported and converted into an *Alpha Shape* (Library for computations regarding 3D bodies), see Figure B.1. The algorithm determines the closest point on the Alpha Shape to a given target point $\mathbf{p} = (p_x, p_y, p_z)$, which is the current location of the leader. The algorithm also computes the vector from the target point to the closest point on the alpha shape for calculating the haptic force. The algorithm is structured as follows:

Is target point inside Alpha Shape?
The algorithm first checks whether the target point lies inside the alpha shape:

- If the target point is classified as `INTERIOR`, the minimum distance is set to zero, and the distance vector remains the zero vector, setting the haptic force to zero.

Iterating Over Facets to Find the Closest Point
If the target point is outside the Alpha Shape, the algorithm iterates over all facets (triangular faces) of the shape:

1. Extracts the three vertices of the triangle.
2. Computes the closest point on the triangle to the target point.
3. Calculates the squared distance between the target point and this closest point.
4. If this distance is smaller than the previously stored minimum distance, it updates the closest point and the minimum distance.

B.3.1. Computing the Distance Vector
Once the closest point $\mathbf{c}$ is determined, the distance vector is computed as:

$$\mathbf{d} = \mathbf{p}_{\text{closest}} - \mathbf{p}$$

This vector represents the shortest displacement from the target point to the alpha shape. The haptic force is calculated based on this displacement.

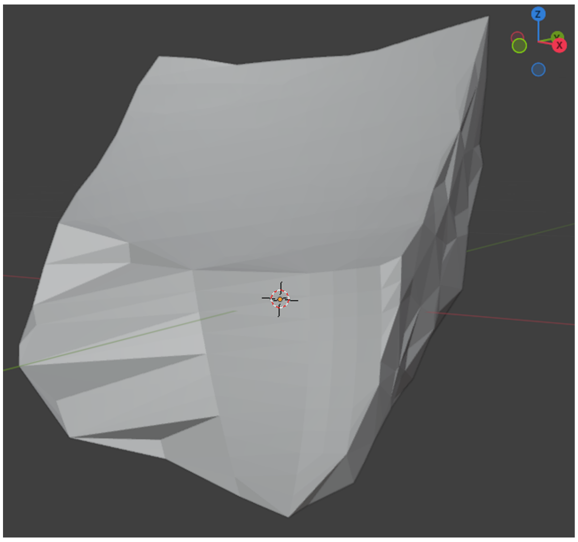

Figure B.1: rendered translational EW

Appendix C

ROS framework

The most important parts of the ROS framework for running the teleoperation setup are presented below.

C.1. Interface

The most important component facilitating communication between the leader and the follower is a ROS node named /kuka_commander. This node serves as the interface, enabling communication between the leader and the follower.

C.2. Sigma.7

The Sigma.7 haptic device sends pose and wrench (force/torque) data to the interface, as illustrated in Figure C.1. The /sigma7_node loads the database containing the translational EW, see Figure B.1

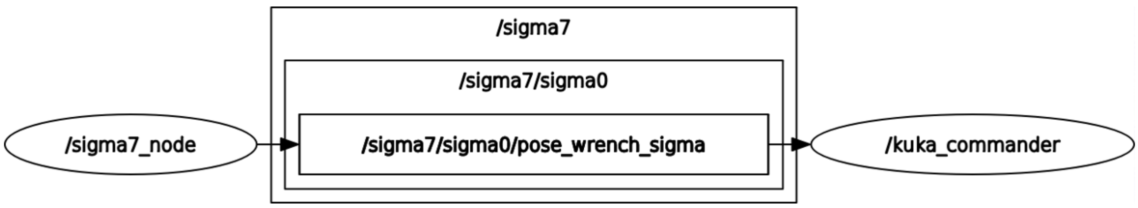

Figure C.1: kuka_commander node receiving Sigma.7 data

C.3. KUKA

/kuka_commander interfaces with the KUKA-controller as shown in Figure C.2. /kuka_commander contains the dynamic reindexing controller that converts sigma movements to references for the KUKA robot.

C.4. Real-time RULA calculation

During teleoperation a Realsense D435 records RGB and depth images of the operator, see Figure C.3. These images are sent to the /pose_detection_node, which determines the keypoints (shoulders, elbow, wrist ...) of the operator. This data is wrapped in a /arm_movement_data message and sent to the /rula_node, which calculates the RULA score for the current ergonomic score of the operator.

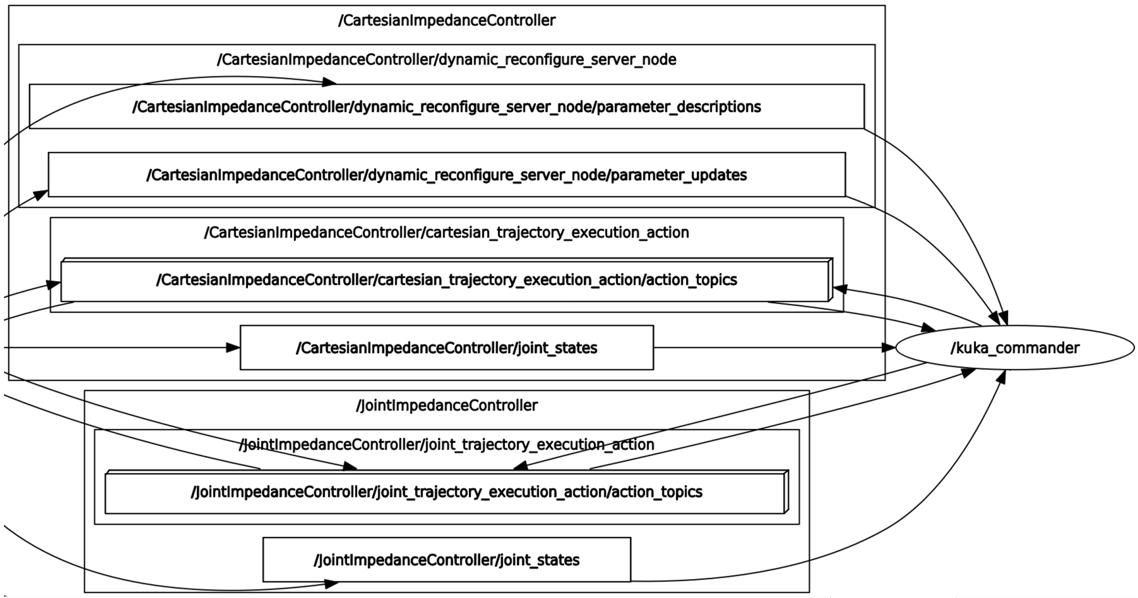

Figure C.2: kuka_commander node interfacing with KUKA

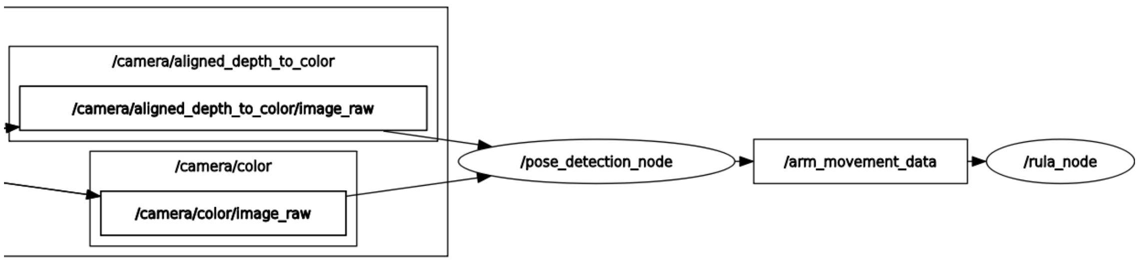

Figure C.3: Realsense data sending to /pose_detection_node. Operator poses are sent to the rula_node.

Appendix D

RULA components

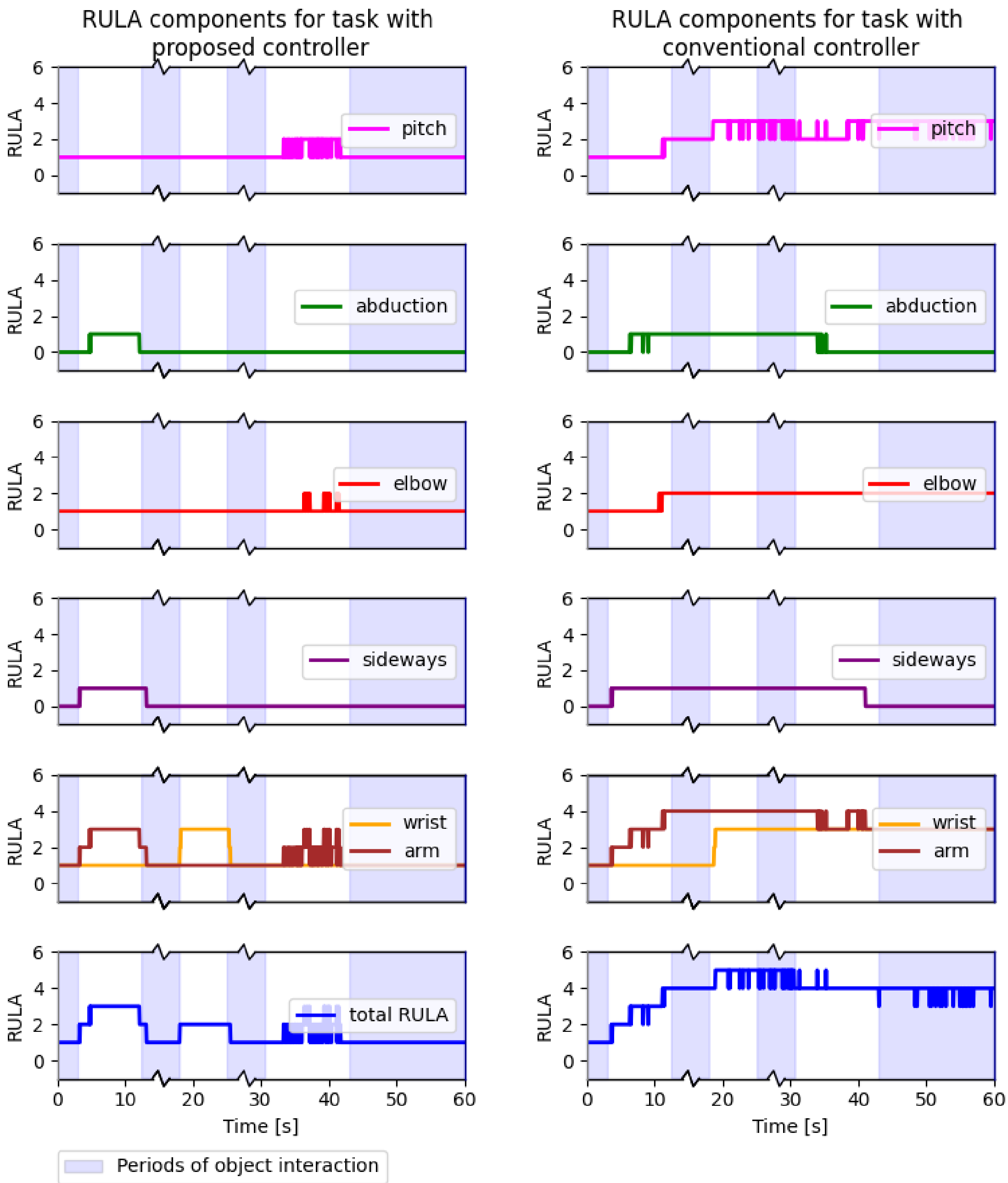

Figure D.1: RULA components during task execution

Appendix E

Body motion based workspace movement

Since the proof-of-concept task was executed under the assumption of no body movement, this Appendix presents preliminary results demonstrating how the EW moves in real-time as the operator moves their body. Figure E.1 shows movement of the EW after the operator rotated its body forward. As a result, the target object is now located inside of the ergonomic workspace.

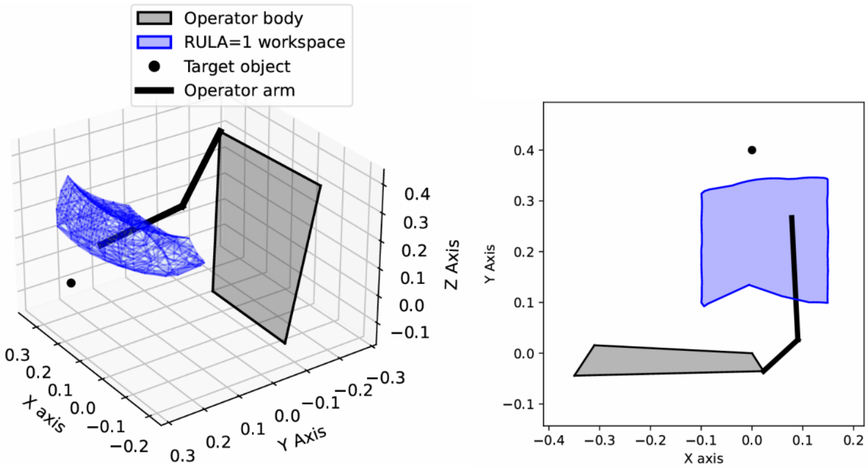

(a) Operator pose with target object beyond reach of the EW. 3D plot on the left, 2D top view on the right.

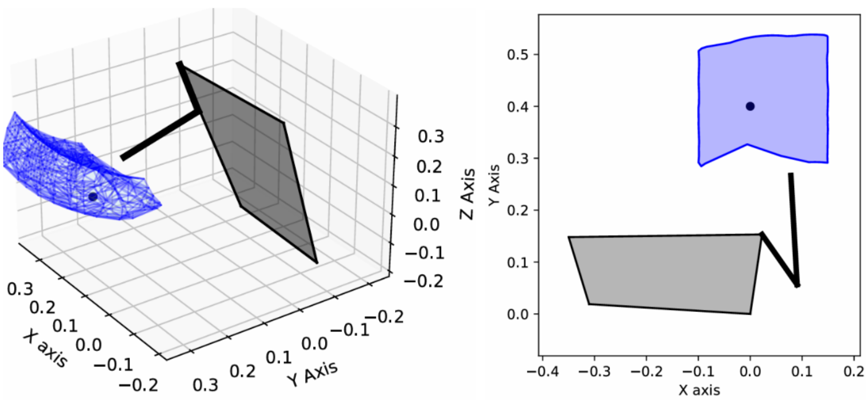

(b) Operator pose after rotating body forward. Note that wrist is still at the same location, but that the EW moved onto the target object

Figure E.1